

Accepted Manuscript

Energetics of melting of Yb_2O_3 and Lu_2O_3 from drop and catch calorimetry and first principles computations

Matthew Fyhrie, Qi-Jun Hong, Denys Kapush, Sergey V. Ushakov, Helena Liu, Axel van de Walle, Alexandra Navrotsky

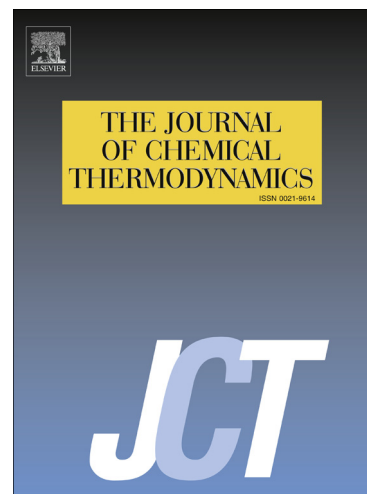
PII: S0021-9614(18)30890-5
DOI: <https://doi.org/10.1016/j.jct.2019.01.008>
Reference: YJCHT 5683

To appear in: *J. Chem. Thermodynamics*

Received Date: 29 August 2018
Revised Date: 7 January 2019
Accepted Date: 9 January 2019

Please cite this article as: M. Fyhrie, Q.-J. Hong, D. Kapush, S.V. Ushakov, H. Liu, A. van de Walle, A. Navrotsky, Energetics of melting of Yb_2O_3 and Lu_2O_3 from drop and catch calorimetry and first principles computations, *J. Chem. Thermodynamics* (2019), doi: <https://doi.org/10.1016/j.jct.2019.01.008>

This is a PDF file of an unedited manuscript that has been accepted for publication. As a service to our customers we are providing this early version of the manuscript. The manuscript will undergo copyediting, typesetting, and review of the resulting proof before it is published in its final form. Please note that during the production process errors may be discovered which could affect the content, and all legal disclaimers that apply to the journal pertain.



Energetics of melting of Yb₂O₃ and Lu₂O₃ from drop and catch calorimetry and first principles computations

Matthew Fyhrrie^a, Qi-Jun Hong^b, Denys Kapush^a, Sergey V. Ushakov^a, Helena Liu^b, Axel van de Walle^b Alexandra Navrotsky^a

^a *Peter A. Rock Thermochemistry Laboratory and NEAT-ORU, University of California Davis, Davis, California 95616*

^b *School of Engineering, Brown University, Providence, RI 02912, USA*

Abstract

The energetics of melting of Yb₂O₃ (T_{fus} 2707 ± 20 K) and Lu₂O₃ (T_{fus} 2762 ± 15 K) were studied experimentally by drop-and-catch (DnC) calorimetry and computationally by *ab initio* molecular dynamic (AI MD) techniques. Fusion enthalpies for Yb₂O₃ (102 ± 10) kJ·mol⁻¹ and Lu₂O₃ (125 ± 10) kJ·mol⁻¹ were derived from the steps in enthalpy increments from DnC experiments performed on liquid and solid samples laser heated in an argon flow. Fusion enthalpy values for Yb₂O₃ and Lu₂O₃ obtained from AI MD computations were 124 ± 2 kJ/mol and 124 ± 3 kJ/mol, respectively. High temperature heat capacity values for solid and liquid phases and volume change on melting were obtained from AI MD. Computed volume change on melting for both oxides is less than 1%, prompting an experimental investigation due to difference with prior experimental results. Experimental results indicate substantial dissolution of oxygen in liquid Lu₂O₃.

ACCEPTED MANUSCRIPT

1. Introduction

Lanthanide-containing compounds have a bevy of applications in fields ranging from biomaterials to fuel cells, electro ceramics, and refractory coatings. The CALPHAD (computation of phase diagrams) method [1; 2; 3] is widely used to streamline development of new metallic alloys. However, there are no examples of its practical application to engineer lanthanide-containing ceramics with required properties. The reason for this is a significant gap in the fidelity of computation of phase equilibria between metallic alloys and ceramics. The success of CALPHAD's application to alloys was aided by the standardization of data for condensed phases of 78 pure elements from Scientific Group Thermodata Europe (SGTE) [4]. SGTE data includes fusion enthalpy for all rare earth elements (Y, Sc, La-Lu). There are no such commonly accepted sets of values for rare earth oxides, mostly due to the lack of reliable experimental and computational data at high temperature.

Zinkevich [5] reviewed all experimental data prior to 2006 on rare earth sesquioxides from 298 K to above the melting points. He relied on experimental data on melting temperatures, fusion enthalpy of Y_2O_3 [6], and on volume change on melting of rare earth oxides to estimate missing fusion enthalpies for all other oxides. A review of the thermodynamic properties of lanthanide and actinide oxides was published by Konings *et al.* in 2014 [7]. They did not rely on volume change measurements but used new thermal analysis data on La_2O_3 [8] in addition to Y_2O_3 values [6] used by Zinkevich. The latest assessment of thermodynamic properties of rare earth sesquioxides was published in 2017 by Zhang and Jung [9]. They took a different approach and derived fusion enthalpies from liquidus slopes in $\text{Al}_2\text{O}_3\text{-RE}_2\text{O}_3$ phase diagrams. The values for fusion enthalpies in the two latest assessments are in substantial disagreement, *e.g.*, 68 vs. 113 $\text{kJ}\cdot\text{mol}^{-1}$ for Lu_2O_3 .

In this work, we applied the recently developed drop-and-catch (DnC) calorimetry technique to measure fusion enthalpies for the two most refractory lanthanide oxides: Lu_2O_3 ($T_m = 2707 \pm 15$) K and Yb_2O_3 ($T_m = 2762 \pm 15$) K. The thermodynamic properties of solid and liquid Lu_2O_3 and Yb_2O_3 were also calculated by *ab initio* molecular dynamic techniques. From recent *in situ* X-ray diffraction measurements, both oxides retain the cubic bixbyite C-type structure up to the melting point [10].

2. Experimental Methods

Yb_2O_3 and Lu_2O_3 powders (0.9999 mass fraction purity, REacton) were used for calorimetry. The sample preparation procedure, the drop-and-catch (DnC) calorimetry technique and instrumentation are covered in detail elsewhere [11; 12]. However a general overview of the technique is provided and the DnC calorimeter is shown schematically in Figure 1. Oxide beads of approximately (2.5-3) mm of each compound are prepared by laser melting from powder. The sample beads are levitated in a splittable nozzle aerodynamic levitator and heated from the top with a CO_2 laser; their surface temperature is monitored by a spectropyrrometer [13]. When the desired temperature is reached, the laser is turned off, the nozzle is split, and the sample is dropped, caught and fully enclosed by splittable copper cavity held at 298 K. The drop distance is ~ 50 mm and drop time is ~ 100 msec. The total mass of the splittable cavity in contact with a sample is ~ 20 g which ensures temperature increase less than 25 K after the catch and allows use of sensitive semiconductor heat flux transducers to record the heat effect upon equilibration of the cavity back to 298 K. In the system used for experiments, laser power and flow rate of gas through the nozzle were manually controlled based on measured temperature and visual observation of levitating beads. The synchronization of laser power-off, split and catch sequence and recording of heat flow trace from calorimeter is provided via National Instrument Labview

and Signal Express software. Heat flow traces starting with solid and liquid Lu_2O_3 in O_2 can be seen in the Appendix.

The following modifications were made to the DnC setup to improve its performance. The distance between the walls of the splittable cavity was increased to 4 mm, the plastic covers around the catch plates were fitted with platinum covers to diffuse heat and prevent damage in the case of a missed catch, and tungsten carbide counterweights were added to improve the balance and ensure consistent catching. After modifications and during the measurements, the calorimeter was recalibrated. In addition to previously used calibration with the heat content of a Cu standard, a new Joule effect calibration procedure was performed with a Setaram E.J.3 unit connected with 4 wires to a 100 Ohm thin film Pt RTD (resistance temperature detector) element (Omega, F3105). The dimensions of thin film RTD employed for calibration (2.5 x 1 mm) are similar to the sample bead and allowed calibration of calorimeter sensitivity between 60 and 300 J and at different locations in the chamber. No systematic variation of sensitivity depending on heat effects within the measured range was observed. However, variations up to 8 % were noted depending on the location of the RTD inside the calorimeter chamber. This calls for possible future improvements of calorimeter chamber design. DnC experiments were initially performed in oxygen flow to avoid possible reduction of the samples. After an unexpectedly large effect of oxygen dissolution in Lu_2O_3 melt was discovered, experiments were repeated in argon flow. The average mass of the beads used in DnC experiments in oxygen was ~60 mg. In an attempt to reduce data scatter the experiments in Ar were performed on larger beads, ~80 mg on average.

DnC approach is not limited by interaction with any container material. However, uniaxial laser heating causes a large thermal gradient in the sample, and this is the primary source of uncertainties. The enthalpy increments measured by DnC are reported vs. surface

temperature of the laser heated bead before the drop. To obtain data on liquids, samples were heated (250-550) K above the melting temperature, depending on the sample weight. When the bead was recovered after the drop and used for a new experiment, it was reweighted on a microbalance to account for sample loss by evaporation. Accuracies of fusion enthalpies derived from the step in DnC curve were estimated as $\pm 10 \text{ kJ}\cdot\text{mol}^{-1}$. This was based on previously performed DnC measurements of fusion enthalpy of Al_2O_3 - the only oxide with melting temperature above 2300 K for which fusion enthalpy was previously measured by several groups [12]. No attempt was made to derive heat capacity data from DnC curves.

3. Computations

We employed first-principles density functional theory (DFT) [14] to model Yb_2O_3 , and Lu_2O_3 . All electronic structures were calculated by the Vienna Ab-initio Simulation Package (VASP) [15], with the projector-augmented-wave (PAW) [16] implementation and the generalized gradient approximation (GGA) for exchange-correlation energy, in the form known as Perdew-Burke-Ernzerhof (PBE) [17]. The valence configuration was $([\text{Kr}]4d^{10}4f^{13}5s^2) 4f^1 5p^6 6s^2$ with cutoff radius of 0.1746 nm (Yb_3) for Yb, $([\text{Kr}]4d^{10}4f^{14}5s^2) 5d^1 5p^6 6s^2$ with cutoff radius of 0.1588 nm (Lu_3) for Lu; for oxygen, the 2s and 2p electrons were relaxed with cutoff radius of 0.0820 nm. This required a plane-wave basis set with the cutoff energy of 400 eV.

The electronic temperature was accounted for by imposing a Fermi distribution of electrons on the energy level density of states. The electronic temperature was set consistently with the ionic temperature. We used automated k-meshes generation with a k-point density of $15^3\cdot\text{\AA}^{-3}$ in the Brillouin zone. First-principles molecular dynamics (MD) techniques were utilized to simulate atomic movements and trajectories. Our recently developed SLUSCHI code[18; 19]

was employed to automate the process. The MD simulations were carried out under a constant number of atoms, pressure and temperature condition (NPT , isothermal-isobaric ensemble) with a time step around 1 fs. The thermostat was conducted under the Nosé-Hoover chain formalism [20; 21]. The barostat was realized by adjusting the volume every 80 steps according to average pressure. Although this did not formally generate an isobaric ensemble, this approach has been shown [18] to provide an effective way to change volume smoothly and to avoid the unphysically large oscillation caused by commonly used barostats in solid phases. MD simulations were performed with 96 RE (RE= Yb, Lu) and 144 O atoms in a periodic cell. The cell size is as large as 15 Å to reduce the finite-size effect. The liquid phase was prepared by heating the solid up to 5000 K (about twice the melting temperature) for 0.5 picoseconds. The liquid was then cooled to the simulation temperature. MD simulations were sufficiently long to achieve convergence. The length of MD trajectory varies from 13 to 29 picoseconds, depending on convergence, but generally, 20 picoseconds were sufficient. On average, computations took about 25,000 CPU hours per data point, which required around two weeks on 64 cores of a computer cluster. The computed cell parameters at high temperatures (Table 1) are within 0.6 % from values recently reported by Pavlik *et al.* [10] which confirms the high fidelity of calculations.

4. Results and Discussion

Enthalpy increments from DnC calorimetry are shown in Figures 2-3, the tables which include the weight of each sample bead and integration for heat flow peaks are included in the Appendix. The results of the computation are summarized in Table 1. The thermodynamic data for Yb_2O_3 and Lu_2O_3 from experiment and computation compared with previous assessments are

discussed below. Due to the significant effect of oxygen dissolution in liquid Lu_2O_3 , only data from experiments in Ar are included in Table 2.

Experimental enthalpies of fusion and effect of oxygen dissolution in the melts

For Yb_2O_3 , measurements in oxygen and argon resulted in $\Delta_{\text{fus}}H^\circ$ values of (97 and 104) $\text{kJ}\cdot\text{mol}^{-1}$ respectively, which are within experimental uncertainty ($\pm 10 \text{ kJ}\cdot\text{mol}^{-1}$). However, a significant atmospheric effect was observed for Lu_2O_3 . Experiments in Ar flow produced $\Delta_{\text{fus}}H^\circ$ value of $(125 \pm 10) \text{ kJ}\cdot\text{mol}^{-1}$, the step in enthalpy curve from measurements in oxygen resulted in $90 \pm 10 \text{ kJ}\cdot\text{mol}^{-1}$ (Figures 2 and 3). Observation of solidification of Lu_2O_3 melt in oxygen flow in the aerodynamic levitator indicated oxygen evolution from the melt on crystallization (Fig. 4) which frequently resulted in an explosion of the beads. Oxygen absorption in Lu_2O_3 melt at high temperature is predicted to be a strongly exothermic process in order to compensate for a significant decrease in entropy of O_2 dissolved in liquid vs. in the gas phase. Endothermic effect of oxygen desorption from the melt on crystallization results in a decrease of enthalpy increments of the sample caught in the liquid state and thus in the smaller step on enthalpy curve. However the details of oxygen absorption were not investigated further.

Computational results and comparisons with previous assessments

Computed $\Delta_{\text{fus}}H^\circ$ for Yb_2O_3 is $(124 \pm 2) \text{ kJ}\cdot\text{mol}^{-1}$, somewhat higher than measured by DnC $(102 \pm 10) \text{ kJ}\cdot\text{mol}^{-1}$. In previous Yb_2O_3 thermodynamic assessments [5; 7; 9], premelting phase transformation from cubic C-type structure into hexagonal (H) phase was assumed. It was not confirmed by recent *in situ* diffraction experiments by Pavlik *et al.* [10]. For comparison purposes, enthalpy of fusion of Yb_2O_3 from previous assessments was taken as a sum of enthalpies for C-H transformation and fusion enthalpies. This results in $\Delta_{\text{fus}}H^\circ$ $106 \text{ kJ}\cdot\text{mol}^{-1}$ for

Yb_2O_3 from Zinkevich [5], (111 ± 8) $\text{kJ}\cdot\text{mol}^{-1}$ from Konings *et al.* [7], and 78 $\text{kJ}\cdot\text{mol}^{-1}$ from Zhang and Jung [9]. The $\Delta_{\text{fus}}H^\circ$ for Yb_2O_3 from Konings *et al.* [7] is in better agreement with computation and within uncertainty of the Zinkevich [5] estimate and our measured value. Computed $\Delta_{\text{fus}}H^\circ$ for Lu_2O_3 (124 ± 3) $\text{kJ}\cdot\text{mol}^{-1}$ is in excellent agreement with our DnC measurements in argon (125 ± 10) $\text{kJ}\cdot\text{mol}^{-1}$. Konings *et al.* [7] estimated (113 ± 10) $\text{kJ}\cdot\text{mol}^{-1}$, which overlaps within assigned uncertainties. Zinkevich [5] and Zhang and Jung [9] values are substantially lower (80.4 and 68) $\text{kJ}\cdot\text{mol}^{-1}$, respectively). The same pattern of agreements and discrepancies are observed for the values for $\Delta_{\text{fus}}S^\circ$ from computation, experiments, and assessments, since values for melting temperatures for Lu_2O_3 and Yb_2O_3 used in this work and in all cited assessments are similar (Table 2).

Computed heat capacities for Lu_2O_3 and Yb_2O_3 at (2100-2500) K are similar (157 and 152) $\text{J}\cdot\text{K}^{-1}\cdot\text{mol}^{-1}$, respectively) and in reasonable agreement with the 125 $\text{J}\cdot\text{K}^{-1}\cdot\text{mol}^{-1}$ value at 2000 K from Konings *et al.* [7]. The latter was obtained from extrapolation of experimental data below 1798 K. However, C_p values computed for liquid Yb_2O_3 and Lu_2O_3 (181 and 183) $\text{J}\cdot\text{K}^{-1}\cdot\text{mol}^{-1}$ are substantially higher than estimates of Koning *et al.* [7] (146 and 152) $\text{J}\cdot\text{K}^{-1}\cdot\text{mol}^{-1}$, respectively.

The volume increase on melting for Yb_2O_3 and Lu_2O_3 from *ab initio* MD is less than 1%. Our previous computations by the same method for Y_2O_3 indicated 3.3% volume increase [11]. This is an intriguing result, as the values differ from prior experimental values. The latest published experimental data on volume change on melting of rare earth sesquioxides is the brief communication to the American Ceramic Society by Granier and Heurtault (1988) [22]. They derived the density for seven liquid lanthanide oxides and for Y_2O_3 from photographs of aerodynamically levitated liquid drops and calculated the values for volume change on melting

using the density of solid oxides estimated from high temperature X-ray diffraction data. They reported a 10.8 % volume increase on melting of Yb_2O_3 and a similar value for Y_2O_3 (11.2 %) [22]. No measurements on Lu_2O_3 have been reported. In the presence of gravity, the shape of aerodynamically levitated liquid depends on its surface tension and is not an ideal sphere but an oblate spheroid. Granier and Heurtault [22] do not mention any corrections for the actual shape of the molten samples. Their approach of deriving density of liquid from dimensions observed from top view photographs assuming ideal spherical shape would lead to systematic overestimation of the volume of the liquid and the volume change on melting. Good agreement of computed lattice parameters and fusion enthalpies with experiments validate our computational result on volume change on melting for all oxides.

5. Summary and Future Directions

Fusion enthalpies for Yb_2O_3 and Lu_2O_3 were measured using drop-and-catch calorimetry and computed by *ab initio* MD techniques. Excellent agreement between experiment and computation was observed for Lu_2O_3 , measured $\Delta_{\text{fus}}H^\circ$ value for Yb_2O_3 is 20 % lower than the computed one. Konings *et al.* [7] assessment for fusion enthalpies is in the best agreement with the present experimental and computational results.

The unexpected finding from the experiments is the substantial effect of oxygen dissolution in Lu_2O_3 melt above 3000 K. While the dissolution of gasses in molten metals was studied and modeled extensively for almost a century [23], the process in oxide melts was seldom addressed [24]. A notable exception is the studies of water and CO_2 dissolution at high pressure in geologically relevant complex oxide melts [25] – volcanic eruptions were proposed to be triggered by heterogeneous water bubbles nucleation in magmas [26].

Computations indicate that volume increase on melting for Lu_2O_3 and Yb_2O_3 is less than 1% - in startling contrast with an estimate for Yb_2O_3 made 30 years ago by Granier and Heurnault [22]. This disagreement discourages using these values for thermodynamic assessments and invites redetermination of volume change on melting for rare earth oxides.

Acknowledgments

The work was supported by the National Science Foundation under Collaborative Research Awards DMR-1835939 (Brown University) and DMR-1835848 (UC Davis) and by Brown University through the use of the facilities at its Center for Computation and Visualization. This work uses the Extreme Science and Engineering Discovery Environment (XSEDE) resource Stampede 2 at the Texas Advanced Computing Center through allocation TG-DMR050013N, which is supported by National Science Foundation grant number ACI-1548562. The authors are grateful to Shmuel Hayun for fruitful discussions and his help with Joule effect calibration of DnC.

References

- [1] R. Otis, Z.-K. Liu, pycalphad: CALPHAD-based Computational Thermodynamics in Python, *Journal of Open Research Software* 5 (2017) dx.doi.org/10.5334/jors.140.
- [2] B. Sundman, U.R. Kattner, M. Palumbo, S.G. Fries, OpenCalphad - a free thermodynamic software, *Integrating Materials and Manufacturing Innovation* 4 (2015) 1. <http://dx.doi.org/10.1186/s40192-014-0029-1>.
- [3] L. Kaufman, Computational thermodynamics and materials design, *CALPHAD: Comput. Coupling Phase Diagrams Thermochem.* 25 (2001) 141-161.
- [4] A.T. Dinsdale, SGTE data for pure elements, *CALPHAD: Comput. Coupling Phase Diagrams Thermochem.* 15 (1991) 317-425.
- [5] M. Zinkevich, Thermodynamics of rare earth sesquioxides, *Progress in Materials Science* 52 (2007) 597-647.
- [6] E.E. Shpil'rain, D.N. Kagan, L.S. Barkhatov, V.V. Koroleva, Measurement of the enthalpy of solid and liquid phases of yttria, *High Temp. - High Pressures* 8 (1976) 183-186.
- [7] R.J.M. Konings, O. Beneš, A. Kovács, D. Manara, D. Sedmidubský, L. Gorokhov, V.S. Iorish, V. Yungman, E. Shenyavskaya, E. Osina, The Thermodynamic Properties of the f-Elements and their Compounds. Part 2. The Lanthanide and Actinide Oxides, *Journal of Physical and Chemical Reference Data* 43 (2014) 013101. <https://aip.scitation.org/doi/abs/10.1063/1.4825256>.
- [8] S.V. Ushakov, A. Navrotsky, Direct measurements of fusion and phase transition enthalpies in lanthanum oxide, *J. Mater. Res.* 26 (2011) 845-847.
- [9] Y. Zhang, I.-H. Jung, Critical evaluation of thermodynamic properties of rare earth sesquioxides (RE = La, Ce, Pr, Nd, Pm, Sm, Eu, Gd, Tb, Dy, Ho, Er, Tm, Yb, Lu, Sc and Y), *Calphad* 58 (2017) 169-203. <http://www.sciencedirect.com/science/article/pii/S0364591617300688>.
- [10] A. Pavlik, S.V. Ushakov, A. Navrotsky, C.J. Benmore, R.J.K. Weber, Structure and thermal expansion of Lu₂O₃ and Yb₂O₃ up to the melting points, *Journal of Nuclear Materials* 495 (2017) 385-391. <http://www.sciencedirect.com/science/article/pii/S0022311517306414>.
- [11] D. Kapush, S. Ushakov, A. Navrotsky, Q.-J. Hong, H. Liu, A. van de Walle, A combined experimental and theoretical study of enthalpy of phase transition and fusion of yttria above 2000 °C using “drop-n-catch” calorimetry and first-principles calculation, *Acta Materialia* 124 (2017) 204-209.
- [12] S.V. Ushakov, A. Shvarev, T. Alexeev, D. Kapush, A. Navrotsky, Drop-and-catch (DnC) calorimetry using aerodynamic levitation and laser heating, *Journal of the American Ceramic Society* 100 (2017) 754-760. <http://dx.doi.org/10.1111/jace.14594>.
- [13] R.A. Felice, The spectropyrometer - a practical multi-wavelength pyrometer, *AIP Conference Proceedings* 684 (2003) 711-716.
- [14] W. Kohn, L.J. Sham, Self-Consistent Equations Including Exchange and Correlation Effects, *Phys. Rev.* 140 (1965) A1133.
- [15] G. Kresse, J. Furthmuller, Efficiency of ab-initio total energy calculations for metals and semiconductors using a plane-wave basis set, *Comp. Mater. Sci.* 6 (1996) 15.
- [16] P.E. Blochl, Projector augmented-wave method, *Phys. Rev. B* 50 (1994) 17953.
- [17] J.P. Perdew, K. Burke, M. Ernzerhof, Generalized Gradient Approximation Made Simple, *Phys. Rev. Lett.* 77 (1996) 3865.
- [18] Q.-J. Hong, A. van de Walle, Solid-liquid coexistence in small systems: A statistical method to calculate melting temperatures, *J. Chem. Phys.* 139 (2013) 094114. 10.1063/1.4819792.
- [19] Q.-J. Hong, A. van de Walle, A user guide for SLUSCHI: solid and liquid in ultra small coexistence with hovering interfaces, *Calphad* 52 (2016) 88-97.

- [20] W.G. Hoover, Canonical dynamics: Equilibrium phase-space distributions, *Physical Review A* 31 (1985) 1695-1697. <https://link.aps.org/doi/10.1103/PhysRevA.31.1695>.
- [21] S. Nosé, A molecular dynamics method for simulations in the canonical ensemble, *Molecular Physics* 52 (1984) 255-268. <https://doi.org/10.1080/00268978400101201>.
- [22] B. Granier, S. Heurtault, Density of liquid rare earth sesquioxides, *J. Am. Ceram. Soc.* 71 (1988) C466-C468.
- [23] A. Sieverts, Absorption of gases by metals, *Z. Metallkd.* 21 (1929) 37-46.
- [24] J.P. Coutures, Pure or complex gas-liquid oxide interactions: fundamental and applied aspects, *Rev. Int. Hautes Temp. Refract.* 16 (1979) 211-224.
- [25] D. Sykes, J.D. Kubicki, A model for water solubility mechanisms in albite melts from infrared spectroscopy and molecular orbital calculations, *Geochim. Cosmochim. Acta* 57 (1993) 1039-1052.
- [26] J.E. Gardner, M.-H. Denis, Heterogeneous bubble nucleation on Fe-Ti oxide crystals in high-silica rhyolitic melts, *Geochim. Cosmochim. Acta* 68 (2004) 3587-3597.
- [27] R.J. Konings, O. Beneš, A. Kovács, D. Manara, D. Sedmidubský, L. Gorokhov, V.S. Iorish, V. Yungman, E. Shenyavskaya, E. Osina, The thermodynamic properties of the f-elements and their compounds. Part 2. The lanthanide and actinide oxides, *Journal of Physical and Chemical Reference Data* 43 (2014) 013101.

Table 1. Lattice constants, density and energies of Yb₂O₃ and Lu₂O₃ from *ab initio* MD computations.

Oxide	T/K (Phase)	MD length /(ps)	CPU /h	a/nm	Density/ (g·cm ⁻³)	Energy/ (eV·atom ⁻¹)
Lu ₂ O ₃	2100 (C)	10	584	1.0483(3)	9.18(1)	-7.915(4)
	2300 (C)	9	449	1.0509(2)	9.11(1)	-7.859(4)
	2500 (C)	14	626	1.0535(4)†	9.04(2)	-7.793(5)
	2500 (L)	25	853	-	8.97(3)	-7.554(3)
	2700 (L)	20	874	-	8.84(3)	-7.494(5)
	2900 (L)	16	646	-	8.66(2)	-7.411(9)
Yb ₂ O ₃	2100 (C)	24	258	1.0530(2)	8.97(4)	-7.904(5)
	2300 (C)	23	263	1.0555(2)	8.90(5)	-7.845(4)
	2500 (C)	43	467	1.0579(2)‡	8.84(5)	-7.785(3)
	2500 (L)	41	585	-	8.80(2)	-7.548(3)
	2700 (L)	43	522	-	8.75(3)*	-7.483(5)
	2900 (L)	43	533	-	8.61(3)	-7.407(5)

† *cf.* measured 1.0592(5) nm [10] ‡ *cf.* measured 1.0647(5) nm [10] * *cf.* estimated 7.94 g·cm⁻³ [22]

Table 2. Thermodynamic data for solid and liquid Yb₂O₃ and Lu₂O₃.

Phase/Property		Method	Reference
C-type Yb₂O₃			
S_{fus}/K	2708	Experimental best value	Zinkevich 2007 [5]
	2707 ±20	Experimental best value	Konings <i>et al.</i> 2014 [27]
	2715	Experimental best value	Zhang & Jung 2017 [9]
$\Delta_{\text{fus}}H^\circ / kJ \cdot \text{mol}^{-1}$	102 ± 10	DnC calorimetry	This work
	124 ± 2	<i>Ab initio</i> MD at 2500 K	This work
	106	Assesment†	Zinkevich 2007 [5]
	111 ±8	Assesment†	Konings <i>et al.</i> 2014 [27]
	78	Assesment†	Zhang & Jung 2017 [9]
$\Delta_{\text{fus}}S^\circ / J \cdot K^{-1} \cdot \text{mol}^{-1}$	38 ±2	Experiment $\Delta H/T_{\text{fus}}$ (2707 K)	This work
	45.8 ±0.4	<i>Ab initio</i> MD $\Delta H/T_{\text{fus}}$ (2707 K)	This work
	39.1	Assesment	Zinkevich 2007 [5]
	41 ±2	Assesment	Konings <i>et al.</i> 2014 [27]
	29.0	Assesment	Zhang & Jung 2017 [9]
$C_p^\circ / J \cdot K^{-1} \cdot \text{mol}^{-1}$	152	<i>Ab initio</i> MD (2100-2500) K	This work
Liq Yb₂O₃			
$C_p^\circ / J \cdot K^{-1} \cdot \text{mol}^{-1}$	181	<i>Ab initio</i> MD (2500-2900) K	This work
	146	Assesment	Konings <i>et al.</i> 2014 [27]
ΔV on melting /%	0.5	<i>Ab initio</i> MD at 2500 K	
	10.8	Experiments in Ar	Granier <i>et al.</i> 1988 [22]
C-type Lu₂O₃			
T_{fus}/K	2763	Experimental best value	Zinkevich 2007 [5]
	2762 ±15	Experimental best value	Konings <i>et al.</i> 2014 [27]
	2783	Experimental best value	Zhang & Jung 2017 [9]
$\Delta_{\text{fus}}H^\circ / kJ \cdot \text{mol}^{-1}$	125 ± 10	DnC calorimetry	This work
	124 ± 3	<i>Ab initio</i> MD at 2500 K	This work
	80.4	Assesment	Zinkevich 2007 [5]
	113 ±10	Assesment	Konings <i>et al.</i> 2014 [27]
	68	Assesment	Zhang & Jung 2017 [9]
$\Delta_{\text{fus}}S^\circ / J \cdot K^{-1} \cdot \text{mol}^{-1}$	45 ±2	Experiment $\Delta H/T_{\text{fus}}$ (2762 K)	This work
	44.9 ±0.5	<i>Ab initio</i> MD $\Delta H/T_{\text{fus}}$ (2762 K)	This work
	29.1	Assesment	Zinkevich 2007 [5]
	41 ±2	Assesment	Konings <i>et al.</i> 2014 [27]
	24.4	Assesment	Zhang & Jung 2017 [9]
$C_p^\circ / J \cdot K^{-1} \cdot \text{mol}^{-1}$	157	<i>Ab initio</i> MD (2100-2500)	This work
Liq Lu₂O₃			
$C_p^\circ / J \cdot K^{-1} \cdot \text{mol}^{-1}$	183	<i>Ab initio</i> MD (2500-2900) K	This work
	152	Assesment	Konings <i>et al.</i> 2014 [27]
ΔS on melting, %	0.8	<i>Ab initio</i> MD at 2500 K	This work

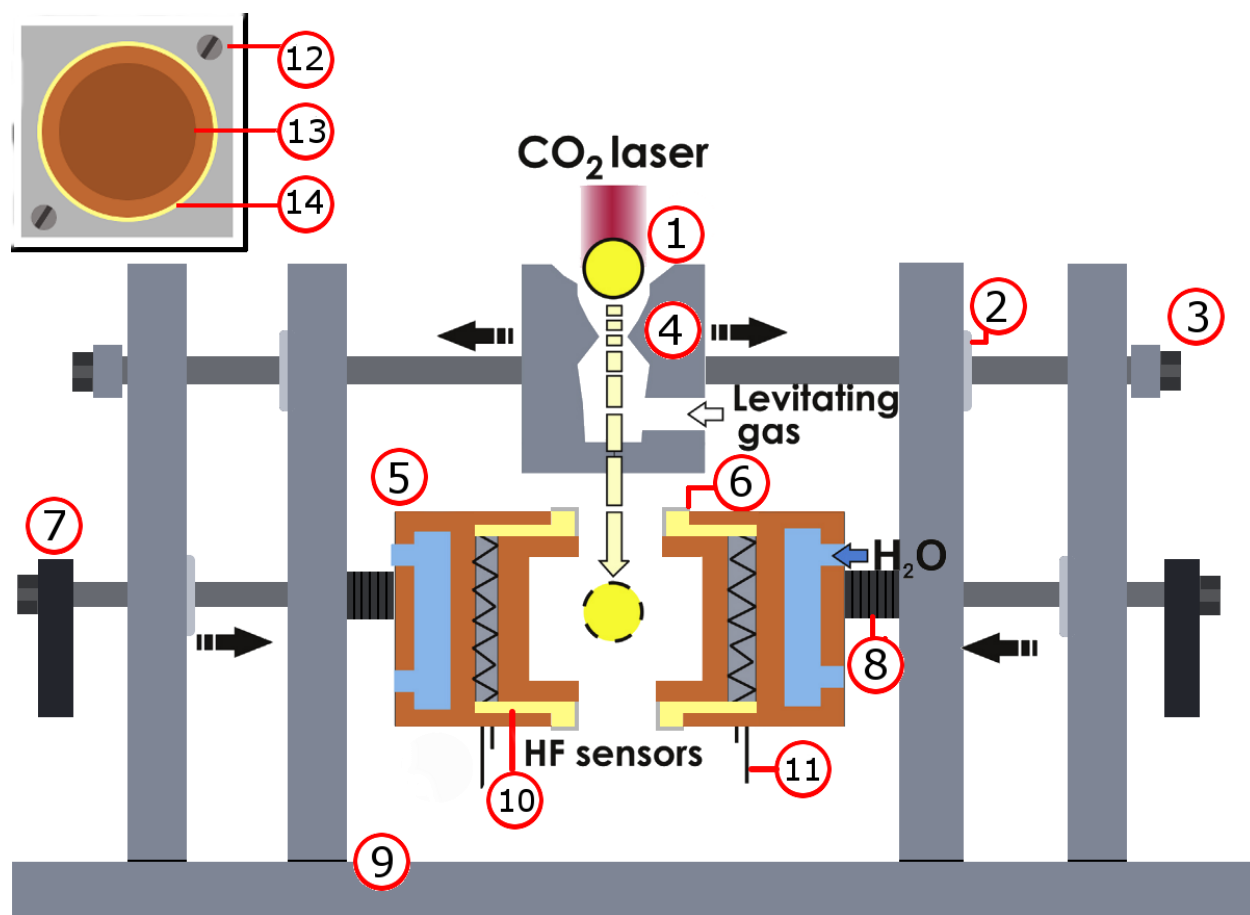
†Calculated as a sum of enthalpies for C-H transformations and fusion

Figure 1. Schematic of the DnC calorimetry system (not to scale): 1 – levitating sample bead; 2 – solenoid for opening and closing levitator, a similar pair is on the support rods for the calorimeter assembly; 3 – end plate for the pair of rods supporting the nozzle; 4 – splittable levitator nozzle; 5 – calorimeter and catch plate assembly; 6 – plastic insulation with overlaying protective platinum cover; 7 – counterweights made of WC; 8 – spacers for fine tuning catch distance; 9 – joint between baseplate and vertical support plates; 10 – insulating spacer between sensor and copper calorimeter body; 11 – sensor wires leading to computer. Calorimeter catch plate front view is shown on the inset in the upper left corner: 12 – platinum covering for plastic insulator cover, held in place by two screws flush with the plastic cover, extending over the top and bottom portions of the plastic; 13 – front view of copper catch plate, the darker portion indicating the cavity; 14 – plastic insulating cover, gap in platinum foil to prevent conducting of heat during catch

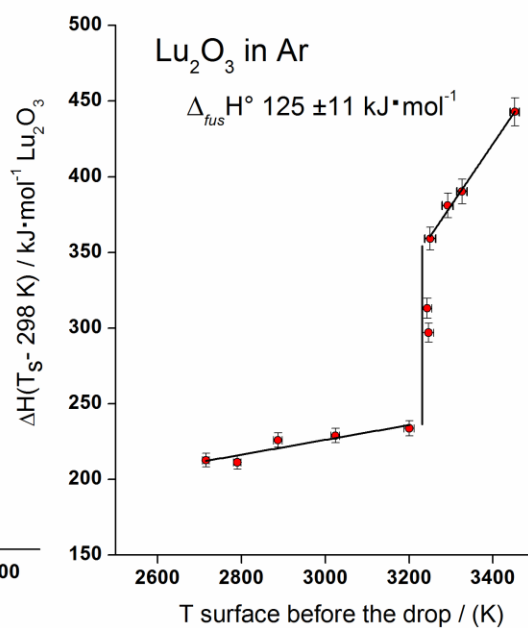
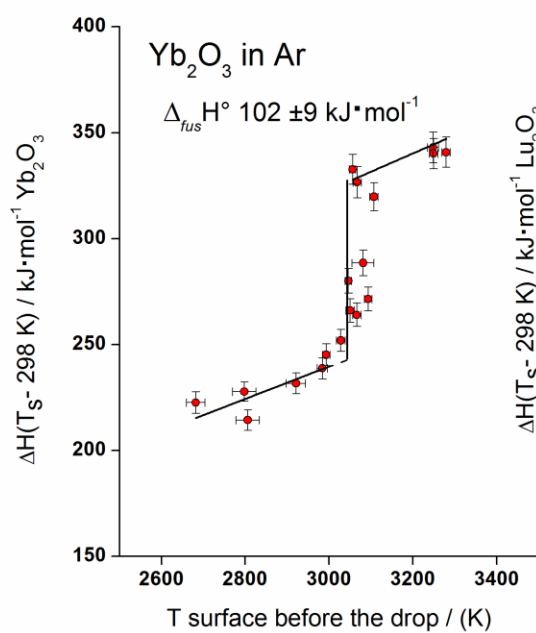
Figure 2. Enthalpy increments measured with DnC calorimeter vs. sample surface temperature before the drops for experiments in Ar. The results for individual data points are tabulated in the Appendix.

Figure 3. Enthalpy increments measured with DnC calorimeter vs. sample surface temperature before the drops for experiments in Ar. The results for individual data points are tabulated in the Appendix.

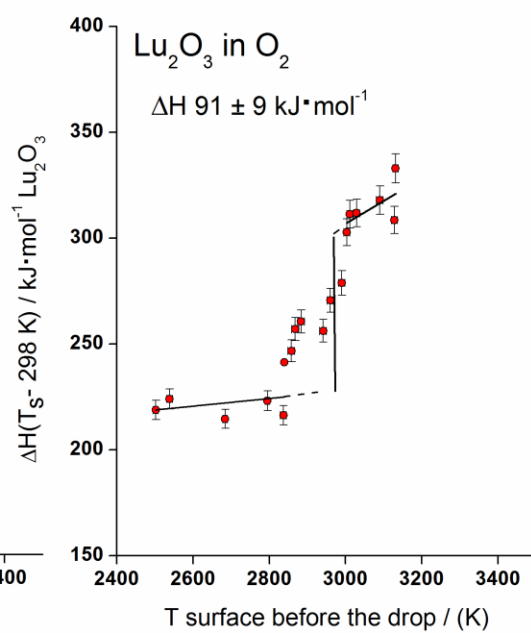
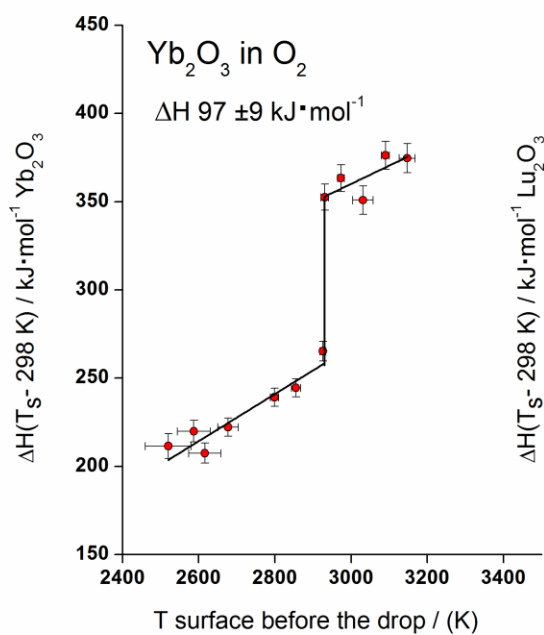
Figure 4. Photographs of Lu₂O₃ solidification after melting in oxygen flow in aerodynamic levitator (A) Lu₂O₃ melt during levitation in oxygen at 3100 K; (B) view of the bead after solidification. The video is included in the Appendix.



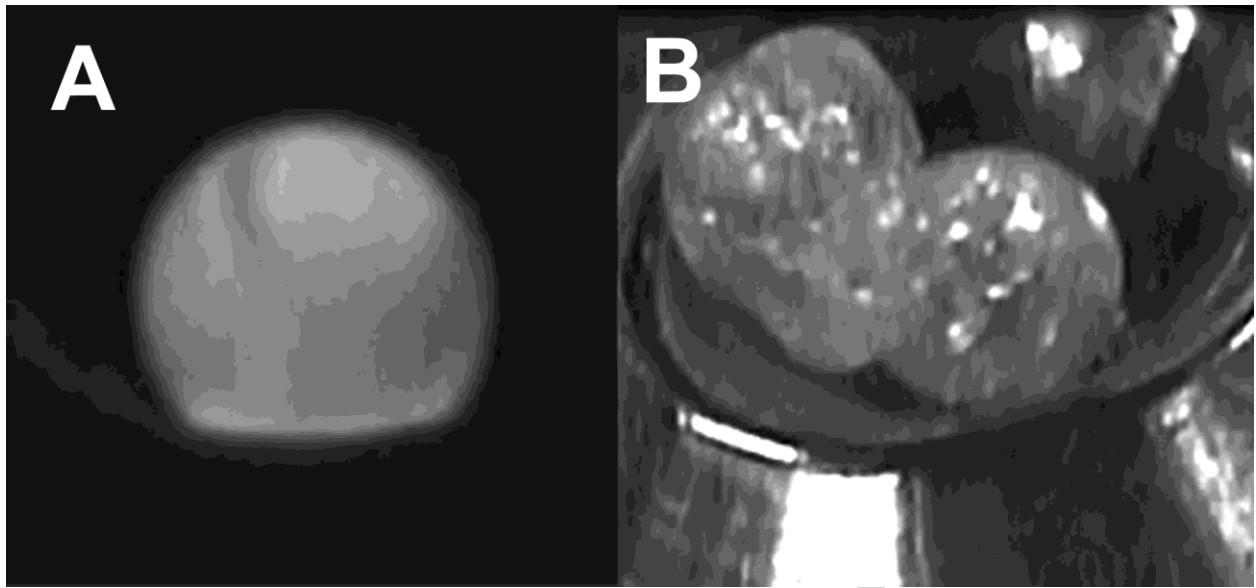
ACCEPTED



ACCEPTED



ACCEPTED



ACCEPTED MANUSCRIPT

- Fusion enthalpies were determined for Yb_2O_3 (102 ± 10 kJ/mol) and Lu_2O_3 (125 ± 10 kJ/mol) using Drop ‘n Catch Calorimetry
- *Ab initio* molecular dynamic computations gave fusion enthalpies of 124 ± 2 kJ/mol and 124 ± 3 kJ/mol for Yb_2O_3 and Lu_2O_3 respectively
- *Ab initio* molecular dynamic computations determined high temperature heat capacity, and volume change on melting for Yb_2O_3 and Lu_2O_3
- Experimental results indicate substantial dissolution of oxygen in liquid Lu_2O_3 , and noticeable atmospheric effect on fusion enthalpy.
- Konings *et al.* 2014 assessment for fusion enthalpies is in the best agreement with the present experimental and computational results.